
MULTI-VIEW MATCHING (MVM): FACILITATING MULTI-PERSON 3D POSE ESTIMATION LEARNING WITH ACTION-FROZEN PEOPLE VIDEO

Yeji Shen

University of Southern California
Los Angeles, CA 90089, USA
yejishen@usc.edu

C.-C. Jay Kuo

University of Southern California
Los Angeles, CA 90089, USA
cckuo@sipi.usc.edu

April 14, 2020

ABSTRACT

To tackle the challenging problem of multi-person 3D pose estimation from a single image, we propose a multi-view matching (MVM) method in this work. The MVM method generates reliable 3D human poses from a large-scale video dataset, called the Mannequin dataset, that contains action-frozen people imitating mannequins. With a large amount of in-the-wild video data labeled by 3D supervisions automatically generated by MVM, we are able to train a neural network that takes a single image as the input for multi-person 3D pose estimation. The core technology of MVM lies in effective alignment of 2D poses obtained from multiple views of a static scene that has a strong geometric constraint. Our objective is to maximize mutual consistency of 2D poses estimated in multiple frames, where geometric constraints as well as appearance similarities are taken into account simultaneously. To demonstrate the effectiveness of 3D supervisions provided by the MVM method, we conduct experiments on the 3DPW and the MSCOCO datasets and show that our proposed solution offers the state-of-the-art performance.

1 Introduction

Human pose estimation is a long-standing problem in computer vision research. It has numerous applications such as sports, augmented reality, motion analysis, visual avatar creation, etc. In the past ten years, a major advance has been made in building large-scale human pose datasets and developing deep-learning-based models for human pose estimation. As a result, estimating multi-person 2D poses and/or a single-person 3D pose in complicated scenes become mature. Yet, multi-person 3D pose estimation is still a challenging problem due to the lack of large-scale high-quality datasets for this application. This is further hindered by inadequate depth estimation algorithms in monocular images.

It is nontrivial to acquire high quality 3D supervisions in dynamic scenes. Depth sensors (e.g., Kinect) can provide useful data, yet the acquisition is typically limited to indoor environments. Furthermore, it often demands a large amount of manual work in capturing and processing. As an alternative, Li *et al.* [1] attempted to estimate dense depth maps using the multi-view stereo (MVS) method from video clips captured in stationary scenes.

The main objective of our current research is to obtain high quality 3D skeletons from multiple 2D poses obtained in each frame of action-frozen people video. Such a dataset was collected by focusing on a special kind of Youtube video. That is, people imitate mannequins and freeze in elaborate and natural poses in a scene while a hand-held camera tours the scene to create the desired video. It is called the Mannequin dataset. This type of video is suitable for human pose estimation since it can provide diverse poses from people of different ages and genders with different scales in a wide variety of outdoor scenes. We propose a multi-view matching (MVM) method to achieve this goal. With a large amount of in-the-wild video data labeled by 3D supervisions automatically generated by MVM, we are able to train a neural network that takes a single image as the input and generate the associated multi-person 3D pose estimation as the output.



Figure 1: Exemplary video clips from the Mannequin dataset, where action-frozen people keep certain poses in diverse environments such as cafe, school, living room, hall, etc.

Our approach has several advantages in multi-person 3D pose estimation. First, the scene does not have to be an indoor and/or lab environment. Second, there are a considerable number of video clips available online. If needed, it is possible to make more action-frozen people video at a low cost. Third, we can get high quality 3D skeleton information by exploiting the static scene assumption. To the best of our knowledge, there is only one in-the-wild 3D human pose dataset, called MPII-3DPW [2]. It relies on Inertial Measurement Unit (IMU) sensors attached to a few actors or actresses. As compared to MPII-3DPW, our approach is more scalable. It contains more diverse contents in terms of subjects and environments. Some exemplary video clips in the Mannequin dataset are shown in Fig. 1. With the help of such video clips, we can obtain diverse 3D human poses in a wide range of scenes in daily life.

Estimating 3D skeletons from predicted 2D poses of multiple views has been studied previously in several settings, e.g. the synchronized multi-camera lab environment [3, 4], the synthesized sports video [5]. However, existing methods do not work well in the current setting (namely, video of action-frozen people captured by a hand-held camera) for the following reason. In the action-frozen video clip, each frame can be essentially regarded as a single view of the scene. A typical 10-second video sequence sampled at 25fps will yield 250 views of the scene from 250 viewing angles. As observed in [3], the main challenge is to build the correspondence of predicted 2D poses in different frames. The optimization method in [3] was developed to minimize the cycle consistency loss in a multi-camera lab environment with a small number of views (e.g. five cameras). The solution in [3] is computationally intractable in our current case, which has a larger number of views and more people in the scene.

Besides, pose tracking methods like [6] can be a potential option when we need to determine which 2D poses in different frames corresponds to the same person. However, we argue that they are also not efficient enough in our case. The reason is that, when identifying the correspondence of multiple 2D poses, the 3D geometric constraints plays a more important role compared to the visual similarity clue that is usually what the pose tracking methods rely on, which is further confirmed by our empirical experiments. As it is not common for pose tracking methods to make assumption of static scenes, the 3D geometric constraints are not fully utilized.

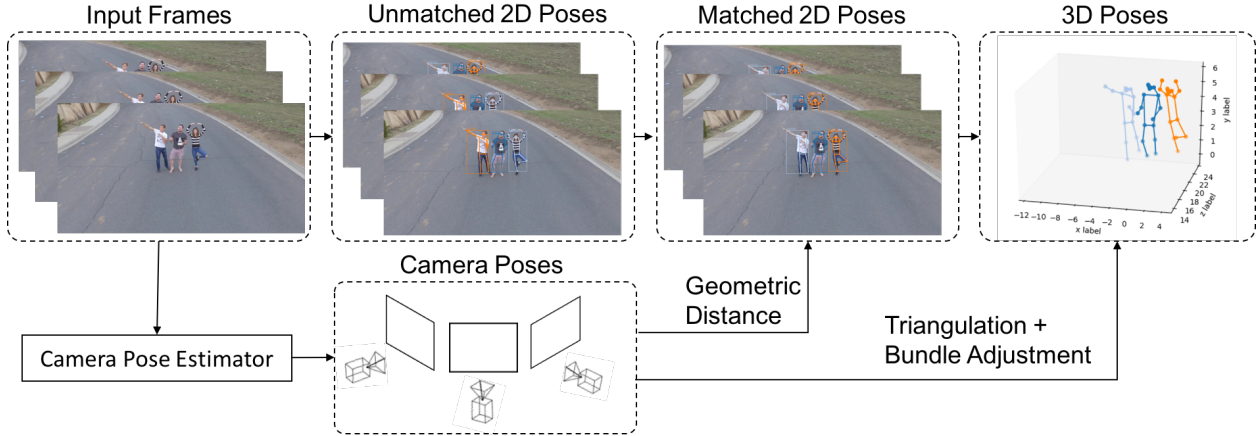


Figure 2: Illustration of the generation of multi-person 3D poses by the proposed MVM method. The input contains a sequence of image frames (shown in the first block), 2D pose estimation at each frame (shown in the second block), building correspondence of 2D poses across multiple frames (shown in the third block), recovering 3D poses from matched 2D poses (shown in the fourth block).

The pipeline of the proposed MVM method is shown in Fig. 2. First, we use the OpenPifPaf method [7] to estimate multi-person 2D poses at each frame. Second, we find the correspondence of 2D poses across multiple frames. This is achieved by adopting an approximation to the optimization objective in [3], where both geometric constraints and appearance similarities are taken into account. Third, we apply triangulation to groups of matched 2D poses and conduct bundle adjustment to recover multi-person 3D poses. We provide both qualitative and quantitative results to show the quality of the multi-person 3D poses in Youtube video.

In practice, we are interested in multi-person 3D pose estimation from a single image. To accomplish this goal, we train a monocular multi-person 3D pose network, which is a modification of the network proposed in [7], from multiple frames using the 3D supervisions obtained by MVM. To demonstrate the effectiveness of 3D supervisions provided by the MVM method, we conduct experiments on the 3DPW and the MSCOCO datasets. Evaluation shows performance improvement in the 3D human pose estimation accuracy for the 3DPW dataset and the 2D human pose estimation accuracy for the MSCOCO dataset.

There are four main contributions of our current research.

- We develop an efficient method, called the MVM method, that leverages geometric constraints and appearance similarities existing in video clips of static scenes. for reliable 3D human poses estimation.
- We collect a large-scale Youtube video clips containing action-frozen people with in-the-wild scenes and call it the Mannequin dataset. It can be used as a training dataset for multi-person 3D pose estimation.
- Although there is no groundtruth, we use the MVM method to generate weak 3D supervisions for the Mannequin dataset so that the dataset can be used to train a multi-person 3D neural network that is applied to a single image.
- We use the Mannequin dataset as the training dataset and show the effectiveness of the weak 3D supervisions provided by MVM through extensive experimental results conducted for the 3DPW dataset and the 2D MSCOCO dataset.

The rest of this paper is organized as follows. Related work is reviewed in Sec. 2. The Mannequin dataset is introduced in Sec. 3. The MVM method is proposed in Sec. 4. The solution to the multi-person 3D pose estimation problem from a single image is discussed in Sec. 5. Experimental results are shown in Sec. 6. Finally, concluding remarks are given in Sec. 7.

2 Review of Related Work

Several previous research related to our current work is reviewed below.

2.1 3D Human Pose Estimation

There are two common representations for 3D human poses: the skeleton-based representation and the parametric-model-based representation. The skeleton-based representation serves as the minimal representation of human poses. It finds applications such as in sports motion analysis [8], among many others. One approach to skeleton-based 3D poses estimation is the use of the 2D-to-3D lifting mechanism. Martinez *et al.* [9] proposed a method that uses a cascade of fully-connected (FC) layers to infer 3D skeletons from 2D skeletons. Recently, Ci *et al.* [10] adopted a modified graph neural network to achieve the same goal. Yang *et al.* [11] proposed a data augmentation method to synthesize virtual candidate poses, which improves performance consistently.

Besides using RGB images as the input, the skeleton-based representation can also be applied to range images for 3D human pose estimation. For example, Marin-Jimenez *et al.* [12] examined a convolutional neural network (CNN) based method that estimates 3D human poses from depth images directly. Zhang *et al.* [13] proposed a clustering based method with hybrid features by integrating the geodesic distance and the superpixel-based mid-level representation.

The parametric-body-model-based representation offers richer information of the human body. Early work used the SCAPE model [14] that fits a body model to annotated 2D keypoints in the image. More recently, the SMPL model [15] becomes popular. Kanazawa *et al.* [16] proposed a method that fits the SMPL model by minimizing the re-projection error with respect to the 2D keypoint annotations while taking the human pose prior such as joint angles and shape parameters into account. Lassner *et al.* [17] included the 2D silhouette projection in the loss function for data with segmentation mask annotations (e.g., the MSCOCO dataset).

Although they are useful in several contexts, both representations cannot be used in our multi-person 3D pose estimation framework directly. For the former, it is not easy to generalize the skeleton model to tackle with a varying number of people in an image. For the latter, the parametric model is too heavy for multi-person 3D pose estimation since it has too many parameters. It is worthwhile to mention that there exists work that targeted at obtaining 3D human poses directly. For example, Papandreou *et al.* [18] showed that a coarse-to-fine volumetric representation is better than the simplest K -by-3 vector representation, where K is the number of keypoints of the skeleton. A similar conclusion was observed in [19], which further proposed an integral regression on 3D skeletons.

2.2 Multi-Person Pose Estimation

To solve the problem of multi-person pose estimation from a single image, we can categorize current methods into two types: the top-down approach [18, 20, 21, 22, 23, 24, 25] and the bottom-up approach [7, 26]. The top-down approach runs a person detector and then estimates body joints in the detected bounding box. The associated methods benefit from advances in person detectors and a vast amount of labeled bounding boxes for people. The ability to leverage the labeled data turns the requirement of a person detector into an advantage. Yet, when multiple bounding boxes overlap, most single-person pose estimators do not work well. Unfortunately, there are many such cases in the Mannequin dataset of our interest so that the top-down approach is not applicable. In contrast with the top-down approach, the bottom-up approach does not rely on a person detector. Kreiss *et al.* [7] first estimated each body joint and, then, grouped them to form a unique pose by a method called the Parts Association Field (PAF).

2.3 Human Pose Tracking

A single-frame multi-person pose estimator cannot ensure consistency of identity across frames. Depending on how multiple frames are utilized, we categorize pose tracking methods into two types: offline methods and online methods. To address the identity correspondence problem across frames, Many offline methods [27, 28, 29, 30] were proposed to enforce temporal consistency of poses in video clips. Since it usually demands the solution of some difficult-to-optimize formula in form of spatio-temporal graphs, their solution speed is slow.

For online methods, a common technique to handle the multi-person identification problem across frames is to maintain temporal graphs in neural networks [31, 32, 33]. Rohit *et al.* [32] proposed a 3D extension of Mask-RCNN, called person tubes, to connect people across time. Yet, its tracking result is no better than the simple baseline Hungarian Algorithm [28] even more time and memory are needed to support the grouped convolution operations in the implementation for a couple of frames. Joint Flow [3] exploited the concept of the Temporal Flow Field to connect keypoints across two frames. However, the flow-based representation suffers from ambiguity when subjects moved slowly (or being stationary). It demands special handling of such cases in the tracking process. Apparently, this method is not applicable to the Mannequin dataset that contains action-frozen people.

2.4 Design Choices of Proposed MVM

In the proposed MVM method, we choose an approximating offline optimization method to balance accuracy and computing efficiency. Furthermore, we choose the bottom-up method since it is a better fit for the context of our interest. Furthermore, we adopt the “2D-skeleton-plus-relative-depth” representation for multi-person 3D pose representation. The above design choices have several advantages. First, unlike most top-down methods which are difficult to generalize to scenes containing a varying number of people in an image, our method can scale from the one-person case to the multi-person case elegantly. Second, both 2D skeletons and their depth information can be expressed using local image coordinates projected to the camera matrix for each corresponding frame independently. This greatly relieves the dependence on camera’s locations. As a result, our multi-person 3D pose estimation network can be trained in the camera-location-independent setting. In other words, our method can work in scenes with simple camera calibration.

3 Mannequin Dataset

# of	Count
Sequences	100
Sampled clips	550
Frames	47263
Unmatched 2D Poses	525901
Matched 2D Poses	176876
Generated 3D Poses	2172
Ave. clips per sequence	5.5
Ave. frames per clip	85.9
Ave. 2D joints per triangulation	41.3

Table 1: Statistics of the Mannequin dataset.

The original Mannequin dataset [1] has around 2000 sequences which consist of around 170K annotated frames with both camera poses and dense depthmaps available. However, some of the video clips are no longer available. We do not need the provided dense depthmaps. To build our own dataset, we manually choose 100 sequences and collect ten clips for each sequence, where each clip is less than 10 seconds. Our dataset consists of 47,263 frames in total. As compared with the original Mannequin dataset, we only use the camera intrinsics information. This is because our re-sampled frames have very few overlaps with the annotated frames in the original sequences and we need to re-compute the camera pose information using the COLMAP method [34] in sampled frames. Unlike the original application of the Mannequin dataset in depth estimation which requires geometric consistency of most pixels in a frame, we only demand consistency of a few pixels corresponding to 2D keypoints. Thus, we have a different criterion in selecting valid frames.

The 100 sequences are chosen such that they contain a large amount of body motion, pose and appearance variations. They also contain severe body part occlusion and truncation. They are attributed to occlusions with other people or objects and the fact that persons may disappear partially or completely and re-appear again. The person scale also varies across the video clip due to camera’s movement. Thus, the number of visible people and body parts varies across a video clip.

4 Multi-View Matching (MVM) Method

The overall pipeline of the proposed 3D multi-view matching (MVM) method is illustrated in 2. For each input clip, we first estimate the camera poses for all frames. Then, a 2D pose estimator is independently applied to those frames to get the initial 2D pose predictions. Next, we run the matching algorithm to find the correspondence of 2D poses across frames. After that, we use triangulation on 2D poses that belong to the same person to get the initial 3D skeleton. Finally, the 3D skeleton is further finetuned by the bundle adjustment algorithm for better consistency of the estimated 3D pose.

4.1 Camera Pose Estimation

By following an approach similar to that adopted by [1] and [35], we use ORB-SLAM2 [36] to identify trackable sequences in each video clip and estimate the initial camera pose for each frame. In this stage, we set the camera intrinsics the same as the one provided in the original Mannequin dataset, and process a lower-resolution version of the video clip for efficiency. Afterwards, we process each sequence at a higher resolution using a visual SfM system [37] to



Figure 3: Visualization of estimated camera poses: exemplary image frames in two video clips (left) and the corresponding estimated camera pose trajectory curves in red (right).

refine initial camera poses and intrinsic parameters. This method extracts and matches features across frames. Then, it conducts the global bundle adjustment optimization. Our implementation is based on an open-sourced multi-view stereo (MVS) system called COLMAP [34]. Two camera pose estimation examples are shown in Fig. 3. We show an exemplary image frame in the left and the estimated camera pose trajectory curve of for the corresponding video clip in red in the right.

4.2 2D Pose Estimation

We use the OpenPifPaf method in [7] as the 2D human pose estimation baseline network. It is trained using results from the keypoint detection task of the MSCOCO dataset. For fair comparison with other similar work in [38] and [39], we adopt a ResNet-152 [40] backbone feature extractor and run the 2D pose estimator on each input frame independently to get the 2D pose predictions x_{ij} along with confidence score $w_{ij} \in [0, 1]$.

4.3 Matching

The objective of this matching step is to determine a set of 2D poses that belong to the same person. This can be mathematically stated as follows. Suppose that there are T frames in a video clip. We use $x_{ij} \in [0, 1]^{C \times 2}$ to indicate the j^{th} 2D pose in the i^{th} frame with C joints for each 2D pose in the normalized image coordinates. For each person k , we would like to determine a group of 2D poses, denoted by

$$G_k = \{x_{i_1 j_1}, x_{i_2 j_2}, \dots, x_{i_{M_k} j_{M_k}}\},$$

that are associated with the same person and M_k is the number of frames this person shows up.

4.3.1 Affinity Matrix

The matching criterion is based on the affinity function, denoted by $A(x_u, x_v)$, of two 2D poses x_u and x_v . The affinity function takes two factors into account; namely, appearance similarity S and geometric distance D . It is expressed as

$$A(x_u, x_v) = S(x_u, x_v) \times \frac{1}{1 + \exp(\gamma D(x_u, x_v))}, \quad (1)$$

where $\frac{1}{1 + \exp(\gamma D)}$ converts a distance measure to a similarity measure and

$$D(x_u, x_v) = \frac{1}{2C} \sum_{c=1}^C d(x_u^c, L_{uv}(x_v^c)) + d(x_v^c, L_{vu}(x_u^c)) \quad (2)$$

is a geometric distance measure between two poses. Furthermore, in Eq. (2), $L_{uv}(x_v^c)$ indicates the epipolar line of the c^{th} joint of 2D pose x from view u to view v and $d(\cdot)$ is the Euclidean distance between a point and a line.

The appearance similarity, $S(x_u, x_v)$, in Eq. (1) is calculated using the cosine similarity of the features extracted from the last conv layer of the network described in Sec. 4.2. The geometric distance, $D(x_u, x_v)$, compute the average distance between the epipolar lines of the 2D keypoints in one frame and the corresponding 2D keypoints in the other frame. The overall affinity is a product of the appearance affinity and the geometric affinity as shown in Eq. (1).

4.3.2 Mutual Consistency Maximization

Suppose that there are N people in total in the entire set of input frames. We use $y_{ij} \in [1..N]$ to indicate the associated person index of pose x_{ij} . Our goal is to maximize the following objective function:

$$\begin{aligned} & \underset{y}{\text{maximize}} && \sum_{k=1}^N \sum_{(i_1, j_1) \in G_k} \sum_{(i_2, j_2) \in G_k} w_{i_1 j_1} w_{i_2 j_2} A(x_{i_1 j_1}, x_{i_2 j_2}), \\ & \text{subject to} && \{G_k\} \text{ is a partition for } \{x_{ij}\}. \end{aligned} \quad (3)$$

In principle, Eq. (3) can be solved by finding the partition of the affinity matrix with the spectral clustering method. However, this classical method is too slow to be practical in our current context. To speed up this optimization process, we develop a greedy algorithm that finds an approximation to the original objective. The main idea is described below in words. The algorithm maintains a set of corresponding 2D poses. It begins with the 2D pose that has the largest confidence from the pool of 2D poses, where the confidence score is generated by the 2D pose network. At each time, we choose the 2D pose with the highest affinity score from the pool, and repeat the process until we cannot find any x_{ij} that has an affinity score above threshold τ . The pseudo codes of the proposed greedy 2D poses matching algorithm are given in Algorithm 1.

Algorithm 1: Pseudo codes for greedy 2D poses matching.

Input : 2D Poses x_{ij} , Affinity Matrix A

Output : G_k for $k \in [1..N]$

Initialize visited set $V = \emptyset$;

for $k \leftarrow 1$ **to** N **do**

Find $x_{i_0 j_0} \notin V$ with the largest confidence;

$G_k \leftarrow \{x_{i_0 j_0}\}$;

Find x_{ij} such that $\sum_{x_{pq} \in G_k} w_{ij} w_{pq} A(x_{ij}, x_{pq})$ is the largest and $i \neq p$ for any $x_{pq} \in G_k$;

while Confidence of x_{ij} is above τ **do**

$G_k \leftarrow G_k \cup x_{ij}$;

Find $x_{ij} \notin V$ such that $\sum_{x_{pq} \in G_k} w_{ij} w_{pq} A(x_{ij}, x_{pq})$ is the largest and $i \neq p$ for any $x_{pq} \in G_k$;

end

$V \leftarrow V \cup G_k$;

end

4.4 Triangulation and Bundle Adjustment

The reconstruction of 3D poses from a group of corresponding 2D poses is a well-studied question in the 3D geometry literature. Here, we use the direct linear transform (DLT) algorithm [41] to estimate the 3D keypoints from multiple

corresponding 2D keypoints. Moreover, we use the RANSAC algorithm to eliminate outliers. The triangulation is applied to different joints independently. Triangulated 3D poses may suffer from small parallax angles, which results in a very large reconstruction error. Some reconstructed poses are even not possible for human beings.

The common practice is to apply bundle adjustment on triangulated 3D poses to get high quality estimates. To implement this idea, we minimize an error function that considers the reprojection error and the human pose prior introduced in [42] jointly. It is formulated by a Gaussian mixture (μ_l, Σ_l) for $l = 1, \dots, 8$ on a dataset of diverse 3D poses [4] in form of

$$\begin{aligned} & \underset{X}{\text{minimize}} && \sum_{x_u} E_R(X, x_u) + \lambda E_P(X), \\ & \text{subject to} && X \in \mathbb{R}^{3 \times C}, \end{aligned} \tag{4}$$

where

$$E_P(X) = -\log \left\{ \sum_{l=1}^8 \mathcal{N}(X|\mu_l, \Sigma_l) \right\}. \tag{5}$$

After we obtain reconstructed 3D poses, we will project them back to each frame to generate a 3D supervision that will be used in the training of a 3D pose estimation network from a single image as discussed in the next section.

5 Multi-Person 3D Pose Estimation from Single Image

5.1 System Overview

In this section, we study how to train a convolutional neural network (CNN) to solve the problem of multi-person 3D pose estimation from a single image. To address this problem, we represent estimated 3D poses with two complementary components: 1) 2D poses and 2) keypoint depths. Our CNN architecture is shown in Fig. 4. It is a variant of a state-of-the-art bottom-up human pose estimation network called PifPaf [7]. It has three key modules:

- a backbone feature extractor (ResNet-152);
- three prediction modules; namely, Parts Intensity Fields (PIF), Parts Association Fields (PAF), and Parts Depths Fields (PDF);
- a 3D pose encoder/decoder.

It is worthwhile to mention that PIF and PAF are the same as [7] while PDF is new. Furthermore, most existing multi-person 3D pose networks, e.g., [42, 43], take multiple frames as the input and perform some sort of 2D-to-3D operations before producing the final 3D poses. In contrast, our network can be trained in an end-to-end manner.

5.2 Key Components

We will discuss the roles and implementations of PIF, PAF, PDF, and the 3D pose encoder and decoder here.

PIF is used to describe where the 2D keypoints are so that the body parts can be localized. Different joints are processed independently. As far as the implementation is concerned, there are 5 components for each location of joint j in the output map. They are c , p_x , p_y , b and σ , where c is the confidence score, (p_x, p_y) denote the coordinates of the point that is closest to joint j , b is used to characterize the adaptive regression loss for (p_x, p_y) , and σ stands for the standard deviation of the Gaussian component at location (p_x, p_y) when we recover the high-resolution confidence map of joint j from a low-resolution output map produced by the network.

PAF is used to characterize the link location of a skeleton, where links are used to connect joints detected by PIF. The joints and links are associated together to form an instance of a skeleton. In our skeleton representation as illustrated in Fig. 5, some PAFs correspond to real bones while others do not. They are just some virtual connections between joints, e.g. the connection between the left ear and the left shoulder. Since both PIF and PAF are the same as those in [7], we refer to the original paper for further details.

PDF is used to regress the relative depth of joints. We use the relative depth because of inherent scale ambiguity of 3D poses recovered from multiple 2D poses. Note that 3D poses used as the groundtruth are expressed in the relative scale. Being similar to PIF, there are 2 PDF components for each location (i, j) . They are d_{ij} and γ_{ij} . The former represents the relative depth at location (i, j) while the latter denotes the radius of the Gaussian component centered at the location of the closest joint, denoted by (p_x^{ij}, p_y^{ij}) . The actual value of the high resolution depth map at location (x, y) satisfies

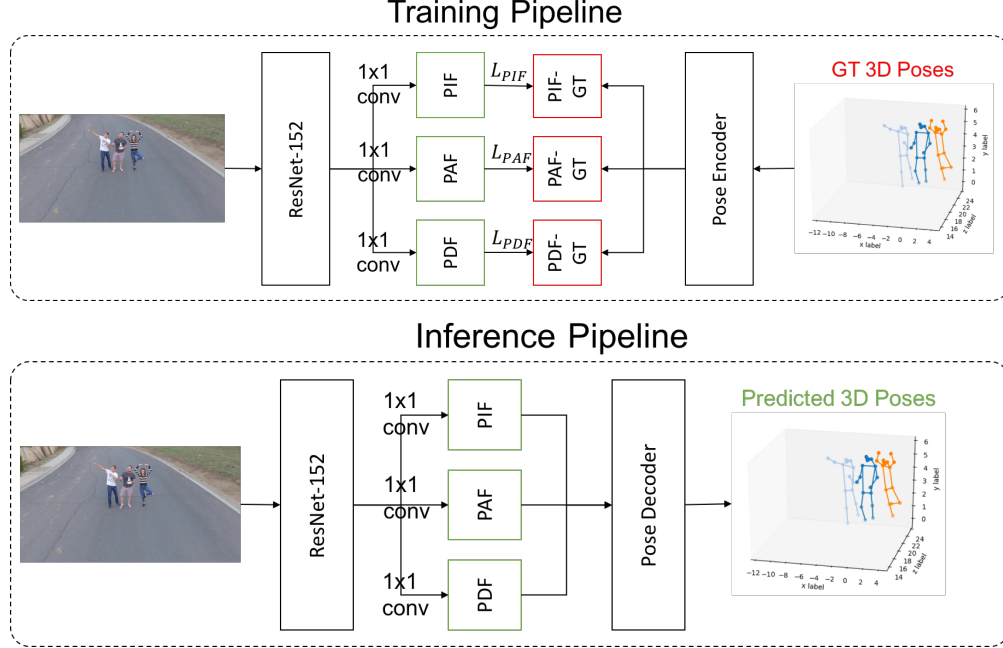


Figure 4: The proposed CNN for multi-person 3D pose estimation from a single image.

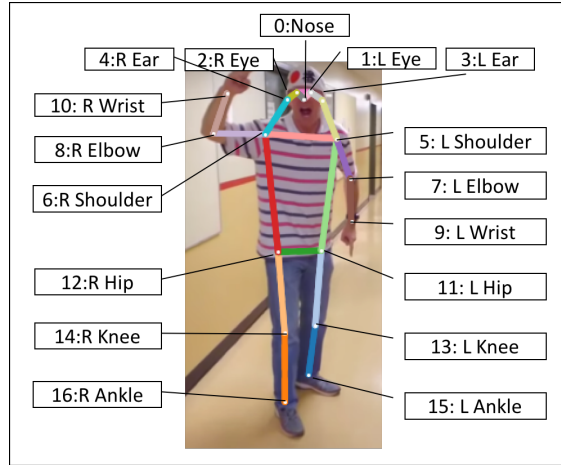


Figure 5: The skeleton representation of human poses in our framework.

the following:

$$D_{xy} = \sum_{i,j} d_{ij} \mathcal{N}(x, y | (p_x^{ij}, p_y^{ij}), \gamma_{ij}). \quad (6)$$

The 3D pose encoder is used to encode three parts fields to the 3D poses while the 3D pose decoder is used to decode the 3D poses to three part fields. As to the 2D poses plus the depth representation of 3D poses, we encoder/decode the 2D pose part in the same way as that is given in [7].

5.3 Loss Function

Since the 3D pose encoder is not differentiable, we need to compute the loss between encoded groundtruth parts fields and the predicted parts fields. The overall loss function is given below:

$$L = \lambda_1 L_{PIF} + \lambda_2 L_{PAF} + \lambda_3 L_{PDF}. \quad (7)$$

Because our camera poses are estimated through the SfM-based method, scale ambiguity is inevitable in our case. To solve the ambiguity problem, we use the following relative depths loss in our network:

$$\begin{aligned} L_{PDF}(d_1, d_2) &= Var[\log \frac{d_1}{d_2}] \\ &= \frac{1}{N} \log \left(\frac{d_1}{d_2} \right)^2 - \frac{1}{N^2} \left(\sum \log \frac{d_1}{d_2} \right)^2. \end{aligned} \quad (8)$$

Therefore, our estimated keypoint depths will try to fit the relative scale of the depth label. It means that the estimated depths and the depth labels are the same if the ratio of these two depths at all locations are consistent.

5.4 Length Scale Calibration

Although the predicted depths are relative, we can still make use of the prior information hidden in human poses to have a rough estimation of the missing scale, s . We need to find s such that the squared difference between the scaled bone length sl_i and the average bone length \bar{l}_i is minimized as given below.

$$\underset{s}{\text{minimize}} \quad \sum_i \frac{1}{2} (sl_i - \bar{l}_i)^2 \quad (9)$$

It is not difficult to show that Eq. (9) has the optimal solution at

$$s^* = \frac{\sum_i \bar{l}_i l_i}{\sum_i l_i^2}. \quad (10)$$

5.5 Network Training

Our proposed CNN for multi-person 3D pose estimation from a single image is shown in Fig. 4. It can be trained by data with incomplete labels, e.g. images with 2D supervisions only, human pose labels with some missing joints. This training flexibility comes from the pose encoder that can generate independent maps for PIF, PAF and PDF separately. If some fields are missing in the ground truth labels, we can simply set the weights of these fields to zero while keeping labels of other fields in the gradient computation process. When training images have 3D supervisions, we project the 3D skeleton information back to the view of each frame so that our network can learn camera-independent multi-person 3D poses.

Before we train the proposed CNN with the Mannequin dataset, we first train it with 64,115 images in the 2017 COCO training set that have 2D pose annotations. In this pre-training process, the PDF branch is not affected since the COCO dataset does not have the depth information. The pre-training of 2D pose related fields can improve the robustness of the ultimate 3D pose estimation network significantly.

In the network training with the Mannequin dataset, we apply the same data augmentation as that is done in [7]. To create uniform batches, we crop images into squares whose side is around 95-100% of the short edge of the image with a randomly selected location. The large crops are done to preserve the size of training images as much as possible. Training images and annotations are horizontally flipped randomly. We use the SGD optimizer with a learning rate of 0.001, momentum of 0.95, a batch size of 8 and no weight decay. We employ model averaging to extract stable models for validation. At each optimization step, we update an exponentially weighted version of the model parameters. The decay constant is 0.001.

6 Experiments

We first conduct experiments to verify the validity of the proposed MVM method quantitatively with the Mannequin dataset. Then, we do performance benchmarking with two public datasets; namely, 3DPW and MSCOCO. The purpose is to show how additional training based on the 3D supervision offered by the proposed MVM method as well as the Mannequin dataset helps improve the performance of the multi-person 3D pose network.

6.1 MVM Evaluation with Mannequin Dataset

We will demonstrate the effectiveness of the proposed MVM method using the Mannequin challenge dataset in both qualitative and quantitative ways. For the qualitative performance of generated 3D poses, some predicted examples are shown in Fig. 6. There are two people sitting on the carpet with severe occluded poses in the first column of this figure.

We see from this example the capability of the proposed MVM method in recovering complicated poses. In some scenarios, we may have a low confidence score of a predicted human pose (e.g. the orange girl in the third column) or a small parallax angle to result in the failure of 3D reconstruction, (e.g., some part of the joints associated with the orange-and-pink person in the second column). The MVM method tends to filter out such instances.

For quantitative evaluations, since the Mannequin dataset does not have any labels, we use the following metric to quantify the validity of generated 3D poses: the reprojection error E_R of estimated 3D poses with their corresponding 2D poses. If the average reprojection error is low enough, it is reasonable to trust quality of the generated 3D poses.

Matching Algorithm	E_R (px) ↓	Outliers ↓	$ G_k $ ↑	E_R (px) w/o RANSAC ↓	$ G_k $ w/o RANSAC
Baseline (Hungarian + MSE)	33.1	12.1	6.5	N/A	18.7
Arnab et al. [42] (Shortest Path w/ MSE)	25.7	3.3	14.7	40.9	18.1
MVM	14.6	8.5	41.2	28.8	49.7
*Dong et al. [3] (Optimization + Our Similarity)	9.6	2.9	10.5	22.3	13.5
*MVM	10.4	5.1	10.8	25.1	15.9

Table 2: Performance comparison between several matching algorithms, where * means only evaluated on clips with less than 50 frames. Otherwise, it would take too much time to run Dong’s algorithm. Smaller reconstruction error E_R implies more consistent 3D poses. A larger number of corresponding 2D keypoints $|G_k|$ as well as a smaller number of outliers means a more robust 3D reconstruction process and thus potentially better 3D poses.

We compare the MVM method with three other methods in Table 2. They are:

1. a baseline that uses sequential matching;
2. a shortest path matching method [42];
3. the state-of-the-art optimization-based matching algorithm [3].

The triangulation is computed joint-wise. We also compare the effect of RANSAC in eliminating outliers. The quantity, $|G_k|$, in the table means the number of the 2D keypoints chosen for triangulation.

As shown in Table 2, the proposed MVM method achieves comparable performance with the state-of-the-art optimization method [3] on short clips at a much lower computational cost. These video clips are short enough for the optimization method to converge within a reasonable amount of time (e.g. an hour). For longer video clips, our MVM method outperforms both the baseline method and the shortest path matching algorithm by a large margin.

	Ave. E_R	Ave. $ G_k $
Shortest Path w/ MSE	25.7	14.7
Shortest Path w/ Geo Dist	20.5	22.6
Shortest Path w/ Geo Dist + Appearance	19.6	19.8
MVM w/ MSE	N/A	15.8
MVM w/ Geo Dist	16.8	45.5
MVM w/ Geo Dist + Appearance (ours)	14.6	41.2

Table 3: Comparison among different affinity matrices.

Furthermore, we show how different similarity metrics affect the quality of generated 3D poses in Table 3. It is clear from the table the proposed geometric distance contributes the most performance gain in terms of the average reprojection error. As to the appearance similarity, although it reduces the total number of matched 2D poses slightly, we can obtain the best overall reprojection error by combining the geometric distance and the appearance similarity since their integration introduces more constraints to matched poses.

6.2 3DPW Evaluation

Very few multi-person 3D human pose datasets are available to the public. One recently released dataset, called the MPII-3DPW [2], contains 60 clips. It contains outdoor video clips captured by a mobile phone with 17 IMUs attached to the subjects. The IMU data allow people to accurately compute 3D poses and use them as the ground truth. The test set consists of 24 video clips. We use the 14 keypoints that are common in both MSCOCO and SMPL skeletons. The same setting was also used in [42]. We evaluate on those frames that have enough visible keypoints for 3D pose estimation and ignore subjects that have less than seven 2D visible keypoints. We compute the Procrustes Aligned

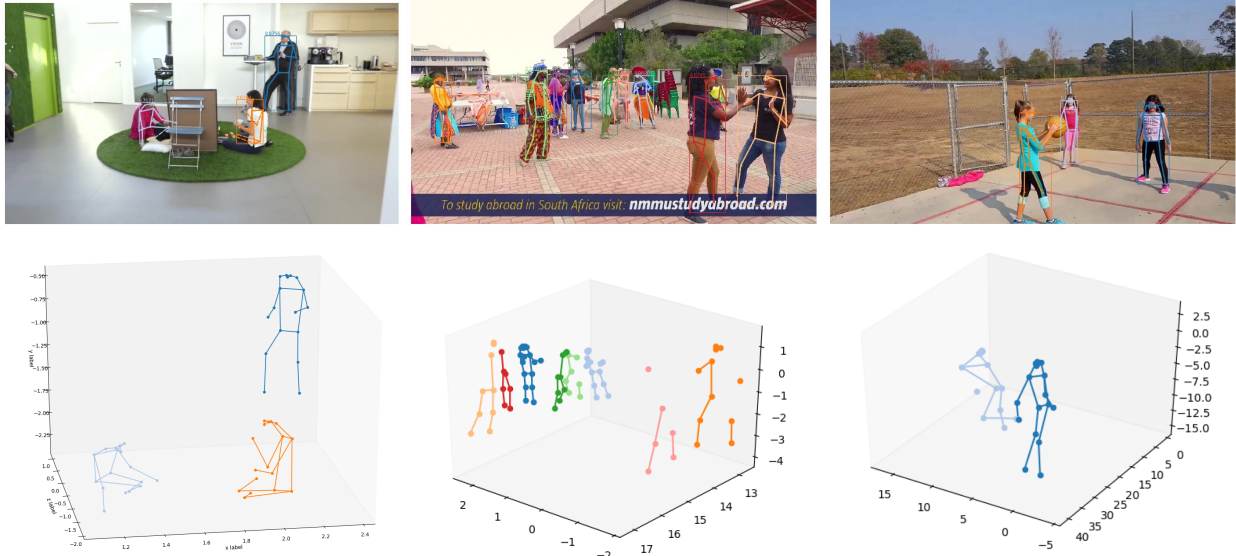


Figure 6: Visualization of the Mannequin dataset results: (1st row) original images with 2D poses, (2nd row) generated 3D poses. The first column indicates a successful estimation of 3D poses in the scene. Due to the low confidence score (e.g., the orange girl in the third column) or a small parallax angle which can cause the failure of 3D reconstruction (e.g., some part of the joints associated with the orange-and-pink person in the second column), the MVM method filters out such instances in a scene.

Mean Per Joint Position Error (PA-MPJPE) [42] independently for each pose and, then, average errors for each tracked person in each video clip. This process implies that we count video clips with two people twice, etc. Finally, we average over the entire dataset.

single frame	PA-MPJPE (mm) ↓
Popa et al. [44]	108.2
SMPLify, Bogo et al. [45]	108.1
Train w/ Our network	82.3
Train + Mannequin dataset w/ our network	78.8
Train w/ HMR [16]	81.3
Train + Mannequin dataset w/ HMR [16]	78.2

Table 4: Evaluation of estimated 3D poses for the MPII-3DPW dataset.

Table 4 shows how incorporating additional data from our Mannequin dataset improves results on 3DPW testing set. Training our proposed network with our data can improve the PA-MPJPE by 3.5mm. Since 3DPW dataset has annotations for the full parametric body model, SMPL model [15], it is expected to have better performance if the network can leverage the such information. Thus, we compare the performance of HMR model trained in 3DPW dataset and the performance trained in 3DPW and Mannequin dataset. The PA-MPJPE was improved by 3.1mm.

6.3 MSCOCO Evaluation

Besides facilitating 3D pose estimation, we are able to improve the accuracy of 2D pose estimation by training a learning system using our Mannequin dataset. Table 5 provides quantitative results for the COCO dataset. The evaluation metrics in COCO dataset are based on the mean average precision (AP) over 10 object keypoint similarity (OKS) thresholds as the main competition metric [46]. The OKS score can measure the similarity between two 2D poses, which essentially serves as a similar role like what IoU does in object detection or segmentation. Our dataset can improve the baseline performance by 1.9 in mAP. The training benefits from the additional data in our dataset which has a lot of weird poses. Apparently, it is more likely for people to make strange and challenging poses in the shooting of a video clip to be uploaded to the Youtube. As a result, our dataset helps recover difficult cases.

	mAP@OKS \uparrow	AP@OKS=0.5 \uparrow
Train	64.6	85.9
Train + Mannequin dataset	66.5	87.1

Table 5: Evaluation of estimated 2D poses in the COCO validation set.

These experiments show how one can effectively use the Mannequin dataset to improve the per-frame 2D pose model in multiple datasets. Besides, in Table 6, we compute C_{var} to empirically compare the consistency of the initial 2D pose estimator. As is defined in Equation 11, C_{var} stands for the variance of pairwise triangulated 3D keypoints of 2D pose predictions,

$$C_{var}(\{x_u^c\}) = \frac{1}{M(M-1)/2} \sum (F_{tri}(x_u^c, x_v^c) - \mu_X^c)^2, \quad (11)$$

where τ is the threshold to eliminate outliers. As shown in the table, OpenPifPaf can produce a more consistent set of 2D poses. This is the reason we used OpenPifPaf as the default 2D pose estimator.

2D pose network	$C_{var}@\tau = 0.5$	$C_{var}@\tau = 0.9$
Mask-RCNN [20]	581.8	233.6
OpenPifPaf [7]	351.0	185.7

Table 6: Comparison between two 2D pose estimation networks, where we report the variance, C_{var} , of the pairwise triangulated 3D poses, which is used to measure consistency of predicted 2D poses, and τ is the threshold to eliminate outliers.

7 Conclusion and Future Work

An MVM method was proposed to generate reliable 3D supervisions from unlabeled action-frozen video in the Mannequin dataset so as to improve the estimation accuracy of multi-person 2D and 3D poses. The MVM method attempts to match 2D human poses estimated across multiple frames. The key to efficient matching lies in taking the geometric constraint (of static scenes in the Mannequin dataset) and appearance similarity into account jointly. Afterwards, through the triangulation of a group of matched 2D poses, optimization by considering the human pose prior and re-projection errors jointly and bundle adjustment, we can obtain reliable 3D supervisions. These 3D supervisions are used to train a multi-person 3D pose network. It was demonstrated by experimental results that both 3D pose estimation accuracy (tested for the 3DPW dataset) and 2D pose estimation accuracy (tested for the MSCOCO dataset) can be improved.

There are several research directions worth further exploration. They are elaborated below.

- Acquiring more information from videos of action-frozen people such as 3D surfaces, textures, etc. In the static scene setting, it is feasible to obtain reliable estimates of various scene information with no manual labels.
- Utilizing weak 3D supervisions obtained from the Mannequin dataset. Although the 3D poses generated by MVM method are accurate, we may have an incomplete number of joints. This is caused by insufficient parallax (viewing angle). To give an example, the right ear might be missing since it is not seen in input frames. One might “inpaint” incomplete pose supervisions to obtain a pseudo groundtruth.
- Utilizing 3D point cloud information when running COLMAP. COLMAP can be used to estimate camera poses and the 3D point cloud information. Currently, we only use the camera pose information. The 3D point cloud set may provide some extra useful information for better 3D pose estimation.

References

- [1] Zhengqi Li, Tali Dekel, Forrester Cole, Richard Tucker, Noah Snavely, Ce Liu, and William T Freeman. Learning the depths of moving people by watching frozen people. In *Proceedings of the IEEE Conference on Computer Vision and Pattern Recognition*, pages 4521–4530, 2019.

- [2] Timo von Marcard, Roberto Henschel, Michael J Black, Bodo Rosenhahn, and Gerard Pons-Moll. Recovering accurate 3d human pose in the wild using imus and a moving camera. In *Proceedings of the European Conference on Computer Vision (ECCV)*, pages 601–617, 2018.
- [3] Junting Dong, Wen Jiang, Qixing Huang, Hujun Bao, and Xiaowei Zhou. Fast and robust multi-person 3d pose estimation from multiple views. In *Proceedings of the IEEE Conference on Computer Vision and Pattern Recognition*, pages 7792–7801, 2019.
- [4] Hanbyul Joo, Tomas Simon, Xulong Li, Hao Liu, Lei Tan, Lin Gui, Sean Banerjee, Timothy Godisart, Bart Nabbe, Iain Matthews, et al. Panoptic studio: A massively multiview system for social interaction capture. *IEEE transactions on pattern analysis and machine intelligence*, 41(1):190–204, 2017.
- [5] Lewis Bridgeman, Marco Volino, Jean-Yves Guillemaut, and Adrian Hilton. Multi-person 3d pose estimation and tracking in sports. In *Proceedings of the IEEE Conference on Computer Vision and Pattern Recognition Workshops*, pages 0–0, 2019.
- [6] Mykhaylo Andriluka, Umar Iqbal, Eldar Insafutdinov, Leonid Pishchulin, Anton Milan, Juergen Gall, and Bernt Schiele. Posetrack: A benchmark for human pose estimation and tracking. In *Proceedings of the IEEE Conference on Computer Vision and Pattern Recognition*, pages 5167–5176, 2018.
- [7] Sven Kreiss, Lorenzo Bertoni, and Alexandre Alahi. Pifpaf: Composite fields for human pose estimation. In *The IEEE Conference on Computer Vision and Pattern Recognition (CVPR)*, June 2019.
- [8] Takuya Ohashi, Yosuke Ikegami, and Yoshihiko Nakamura. Synergetic reconstruction from 2d pose and 3d motion for wide-space multi-person video motion capture in the wild. *arXiv preprint arXiv:2001.05613*, 2020.
- [9] Julieta Martinez, Rayat Hossain, Javier Romero, and James J Little. A simple yet effective baseline for 3d human pose estimation. In *Proceedings of the IEEE International Conference on Computer Vision*, pages 2640–2649, 2017.
- [10] Hai Ci, Chunyu Wang, Xiaoxuan Ma, and Yizhou Wang. Optimizing network structure for 3d human pose estimation. In *Proceedings of the IEEE International Conference on Computer Vision*, pages 2262–2271, 2019.
- [11] Jingjing Yang, Lili Wan, Wanru Xu, and Shenghui Wang. 3d human pose estimation from a single image via exemplar augmentation. *Journal of Visual Communication and Image Representation*, 59:371–379, 2019.
- [12] Manuel J Marin-Jimenez, Francisco J Romero-Ramirez, Rafael Muñoz-Salinas, and Rafael Medina-Carnicer. 3d human pose estimation from depth maps using a deep combination of poses. *Journal of Visual Communication and Image Representation*, 55:627–639, 2018.
- [13] Wenhui Zhang, Dehui Kong, Shaofan Wang, and Zhiyong Wang. 3d human pose estimation from range images with depth difference and geodesic distance. *Journal of Visual Communication and Image Representation*, 59:272–282, 2019.
- [14] Dragomir Anguelov, Praveen Srinivasan, Daphne Koller, Sebastian Thrun, Jim Rodgers, and James Davis. Scape: shape completion and animation of people. In *ACM SIGGRAPH 2005 Papers*, pages 408–416. 2005.
- [15] Matthew Loper, Naureen Mahmood, Javier Romero, Gerard Pons-Moll, and Michael J Black. Smpl: A skinned multi-person linear model. *ACM transactions on graphics (TOG)*, 34(6):1–16, 2015.
- [16] Angjoo Kanazawa, Michael J Black, David W Jacobs, and Jitendra Malik. End-to-end recovery of human shape and pose. In *Proceedings of the IEEE Conference on Computer Vision and Pattern Recognition*, pages 7122–7131, 2018.
- [17] Christoph Lassner, Javier Romero, Martin Kiefel, Federica Bogo, Michael J Black, and Peter V Gehler. Unite the people: Closing the loop between 3d and 2d human representations. In *Proceedings of the IEEE conference on computer vision and pattern recognition*, pages 6050–6059, 2017.
- [18] George Papandreou, Tyler Zhu, Nori Kanazawa, Alexander Toshev, Jonathan Tompson, Chris Bregler, and Kevin Murphy. Towards accurate multi-person pose estimation in the wild. In *Proceedings of the IEEE Conference on Computer Vision and Pattern Recognition*, pages 4903–4911, 2017.
- [19] Xiao Sun, Bin Xiao, Fangyin Wei, Shuang Liang, and Yichen Wei. Integral human pose regression. In *Proceedings of the European Conference on Computer Vision (ECCV)*, pages 529–545, 2018.
- [20] Kaiming He, Georgia Gkioxari, Piotr Dollár, and Ross Girshick. Mask r-cnn. In *Proceedings of the IEEE international conference on computer vision*, pages 2961–2969, 2017.
- [21] Alexander Toshev and Christian Szegedy. Deeppose: Human pose estimation via deep neural networks. In *Proceedings of the IEEE conference on computer vision and pattern recognition*, pages 1653–1660, 2014.
- [22] Guoqiang Wei, Cuiling Lan, Wenjun Zeng, and Zhibo Chen. View invariant 3d human pose estimation. *IEEE Transactions on Circuits and Systems for Video Technology*, 2019.

- [23] Guanghan Ning, Zhi Zhang, and Zhiquan He. Knowledge-guided deep fractal neural networks for human pose estimation. *IEEE Transactions on Multimedia*, 20(5):1246–1259, 2017.
- [24] Jialin Yu, Jifeng Sun, Zhiguo Song, Shaoyin Zheng, and Bingtian Wei. Monocular three-dimensional human pose estimation using local-topology preserved sparse retrieval. *Journal of Electronic Imaging*, 26(3):033008, 2017.
- [25] Xixia Xu, Qi Zou, and Xue Lin. Multi-person pose estimation with enhanced feature aggregation and selection. *arXiv preprint arXiv:2003.10238*, 2020.
- [26] Zhe Cao, Tomas Simon, Shih-En Wei, and Yaser Sheikh. Realtime multi-person 2d pose estimation using part affinity fields. In *Proceedings of the IEEE Conference on Computer Vision and Pattern Recognition*, pages 7291–7299, 2017.
- [27] Eldar Insafutdinov, Mykhaylo Andriluka, Leonid Pishchulin, Siyu Tang, Evgeny Levinkov, Bjoern Andres, and Bernt Schiele. Arttrack: Articulated multi-person tracking in the wild. In *Proceedings of the IEEE conference on computer vision and pattern recognition*, pages 6457–6465, 2017.
- [28] Umar Iqbal, Anton Milan, and Juergen Gall. Posetrack: Joint multi-person pose estimation and tracking. In *Proceedings of the IEEE Conference on Computer Vision and Pattern Recognition*, pages 2011–2020, 2017.
- [29] Bin Xiao, Haiping Wu, and Yichen Wei. Simple baselines for human pose estimation and tracking. In *Proceedings of the European conference on computer vision (ECCV)*, pages 466–481, 2018.
- [30] Weichen Zhang, Lifeng Shang, and Antoni B Chan. A robust likelihood function for 3d human pose tracking. *IEEE Transactions on Image Processing*, 23(12):5374–5389, 2014.
- [31] Andreas Doering, Umar Iqbal, and Juergen Gall. Joint flow: Temporal flow fields for multi person tracking. *arXiv preprint arXiv:1805.04596*, 2018.
- [32] Rohit Girdhar, Georgia Gkioxari, Lorenzo Torresani, Manohar Paluri, and Du Tran. Detect-and-track: Efficient pose estimation in videos. In *Proceedings of the IEEE Conference on Computer Vision and Pattern Recognition*, pages 350–359, 2018.
- [33] Suman Sedai, Mohammed Bennamoun, and Du Q Huynh. A gaussian process guided particle filter for tracking 3d human pose in video. *IEEE Transactions on Image Processing*, 22(11):4286–4300, 2013.
- [34] Johannes L Schönberger, Enliang Zheng, Jan-Michael Frahm, and Marc Pollefeys. Pixelwise view selection for unstructured multi-view stereo. In *European Conference on Computer Vision*, pages 501–518. Springer, 2016.
- [35] Tinghui Zhou, Richard Tucker, John Flynn, Graham Fyffe, and Noah Snavely. Stereo magnification: Learning view synthesis using multiplane images. *arXiv preprint arXiv:1805.09817*, 2018.
- [36] Raul Mur-Artal and Juan D Tardós. Orb-slam2: An open-source slam system for monocular, stereo, and rgb-d cameras. *IEEE Transactions on Robotics*, 33(5):1255–1262, 2017.
- [37] Johannes L Schonberger and Jan-Michael Frahm. Structure-from-motion revisited. In *Proceedings of the IEEE Conference on Computer Vision and Pattern Recognition*, pages 4104–4113, 2016.
- [38] Nikos Kolotouros, Georgios Pavlakos, Michael J Black, and Kostas Daniilidis. Learning to reconstruct 3d human pose and shape via model-fitting in the loop. In *Proceedings of the IEEE International Conference on Computer Vision*, pages 2252–2261, 2019.
- [39] Muhammed Kocabas, Nikos Athanasiou, and Michael J Black. Vibe: Video inference for human body pose and shape estimation. *arXiv preprint arXiv:1912.05656*, 2019.
- [40] Kaiming He, Xiangyu Zhang, Shaoqing Ren, and Jian Sun. Identity mappings in deep residual networks. In *European conference on computer vision*, pages 630–645. Springer, 2016.
- [41] Richard Hartley and Andrew Zisserman. *Multiple view geometry in computer vision*. Cambridge university press, 2003.
- [42] Anurag Arnab, Carl Doersch, and Andrew Zisserman. Exploiting temporal context for 3d human pose estimation in the wild. In *Proceedings of the IEEE Conference on Computer Vision and Pattern Recognition*, pages 3395–3404, 2019.
- [43] Fuyang Huang, Ailing Zeng, Minhao Liu, Qiuxia Lai, and Qiang Xu. Deepfuse: An imu-aware network for real-time 3d human pose estimation from multi-view image. *arXiv preprint arXiv:1912.04071*, 2019.
- [44] Alin-Ionut Popa, Mihai Zanfir, and Cristian Sminchisescu. Deep multitask architecture for integrated 2d and 3d human sensing. In *Proceedings of the IEEE Conference on Computer Vision and Pattern Recognition*, pages 6289–6298, 2017.

- [45] Federica Bogo, Angjoo Kanazawa, Christoph Lassner, Peter Gehler, Javier Romero, and Michael J Black. Keep it smpl: Automatic estimation of 3d human pose and shape from a single image. In *European Conference on Computer Vision*, pages 561–578. Springer, 2016.
- [46] Tsung-Yi Lin, Michael Maire, Serge Belongie, James Hays, Pietro Perona, Deva Ramanan, Piotr Dollár, and C Lawrence Zitnick. Microsoft coco: Common objects in context. In *European conference on computer vision*, pages 740–755. Springer, 2014.